RADIOMETRIC COMPENSATION FOR PROCAM SYSTEM BASED ON ANCHORING THEORY

Ting-Chun Wang[1], Tai-Hsiang Huang[2], and Homer H. Chen[1,2]
[1]Department of Electrical Engineering [2]Graduate Institute of Communication Engineering
National Taiwan University

ABSTRACT

For a procam system consisting of a projector and a camera, the chroma distortion of an image projected on a non-white surface can be compensated by increasing the intensity of the complementary color of the projection surface. However, this inevitably trades image brightness for chroma correctness because the required intensity often outreaches the projector's dynamic range. In this paper, we propose a solution for the compensation problem using the anchoring theory of lightness perception. A notable feature of our technique is that it takes the chromatic adaptation and viewing condition into account, which leads to a better characterization of the image quality perceived by human eyes. As a result, the compensated image appears much closer to the original image. A computational framework for the tradeoff between brightness and chroma distortion is derived, and the performance of the proposed algorithm is verified by subjective experiments.

1. INTRODUCTION

Recently, the projector technology has made significant progress, making possible projections on non-ideal surfaces. To correct the color distortion of an image projected on a colored surface, a camera can be incorporated into a projector to form a closed loop system known as procam.

To counteract the chroma distortions, conventional methods [1]-[3] increase the intensity of the complementary color of the screen. However, the dynamic range of the projector is limited, so the intensity outside the dynamic range will be clipped. To solve this problem, algorithms using multi-projectors have been developed [4]-[5]. However, this solution results in a significant increase of system complexity and cost. The PRISM method [6] utilizes the properties of human visual system (HVS) to achieve brightness uniformity while preserving brightness and contrast; however, it is not content-aware and does not fully utilize the dynamic range of the projector. To better solve it, methods that scale down the image luminance prior to compensation have been proposed [7]-[13]. However, since human eyes have a nonlinear response to luminance, such linear scaling degrades the projection quality.

Unlike previous scaling methods, our algorithm exploits the anchoring theory to cope with the nonlinear properties of HVS. Since color perception depends not only on stimuli themselves but also on the chroma adaptation and the viewing condition, this approach generates results perceptually consistent with the original images.

The remaining paper is organized as follows. The procam model and the anchoring theory are described in Section 2. Section 3 presents the proposed algorithm. The experimental results are given in Section 4. Finally, Section 5 draws the conclusion.

2. REVIEW

In the context of the problem addressed in this paper, the procam system consists of a projector, a camera, and a computer. After the projector projects an image on a colored projection surface, the camera captures the image and sends it to the computer, which modifies the input image and outputs the resulting image to the projector for projection. The goal is to compensate for the effect of the colored screen on the image so that it would look as if it were projected on a white screen.

2.1. Procam Model

Nayar's procam model [1] is often adopted to describe the conversion all the way from the input intensity to the final luminance of an image projected on a screen. With this model, a radiometric compensation process [13] consists of two key steps. First the luminance R on the white screen is estimated from the input intensity I of the original image by $R = P_W(I)$, where P denotes the intensity-to-luminance mapping function and the subscript W refers to the case where the parameters of the function are derived from the white screen. Then, the compensated image I' is determined subject to the constraint $P_C(I') = P_W(I)$, where C denotes that the parameters of the mapping function are derived from the colored screen. This leads to $I' = P_C^{-1}(P_W(I))$. Ideally, the above procedure should work. In practice, however, issues related to the dynamic range of the projector and the nonlinear characteristics of HVS arise and deserve a close investigation.

2.2. Anchoring Theory

Luminance is an absolute quantity measured by equipment. Lightness, on the other hand, is a property that is related to the subjective brightness perception of a color. It belongs to

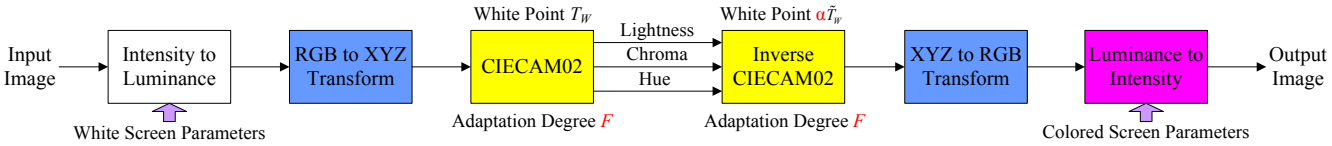

Fig. 1. Block diagram of the proposed algorithm. The red symbols denote the unknowns to be solved via an optimization process.

a broader family called appearances [14], which describe humans' perception of a color. Unlike physical values, appearances are determined with respect to an "anchoring point" in the scene, which is most likely to be the point of the highest luminance [15]. When we look at an object, we actually perceive its appearances instead of its physical values. For this reason, the color of a lamp emitting the same intensity of light in darkness may look different when it is placed under sunlight since the "anchors" in these two scenes are different. It is commonly believed that humans first identify the brightest point in a scene to be "white" and then determine the appearances of other points according to their relationships to the white.

3. PROPOSED ALGORITHM

The proposed gamut mapping algorithm based on the anchoring theory involves the operation of color transform with respect to an anchor and works as follows. First the original anchor is identified and the desired new anchor is computed. Then a color transform that calculates the appearances of the other colors with respect to the original anchor is performed. Finally the inverse color transform with respect to the new anchor is applied to these appearances. This series of operations attempts to reserve the appearances of an image under a new viewing condition, which is associated with a new anchor. This section describes the details of these operations.

There are two gamut mappings in the proposed method—brightness scaling and hue adjustment. The first one scales down the input luminance to within the desired dynamic range, while the second one shifts the input chroma toward the color of the screen. The overall block diagram is shown in Fig. 1. The appearances of the colors are computed according to the CIECAM02 model [16], the latest color appearance model ratified by the CIE Technical Committee. The white point in this model is the anchor in this work.

3.1. Brightness Scaling

In this operation, first the intensities of the input image are transformed to luminance values on the white screen using the intensity-to-luminance function $P_W(\bullet)$ described in Section 2.1, which can be obtained as in [13]. Then they are normalized and transformed to tristimulus values. Next the largest of them T_W is identified, and the CIECAM02 model is applied to the tristimulus values using T_W as the white point to derive their appearances. Finally, these appearances are transformed back to luminance values with respect to a new white point αT_W, where α is a constant that is determined through an optimization process.

3.2. Hue Adjustment

Furthermore, since the screen color would also have effect on humans' perception when they look at a projected image, it may not be necessary to compensate the image to truly white but a little toward the screen color instead. In fact, the truly white on a red screen, for example, may seem a bit green to most humans. In addition, by making the color of the projected image slightly toward the color of the screen, the required intensity of the complementary color can be reduced, leaving more room between it and the upper bound of the projector's dynamic range, so the image brightness can be enhanced.

The implementation is as follows. First the intensities of the input image are transformed to appearances as before. Next $P_C(\bullet)$ is applied to the largest intensity of the input image to obtain its luminance on the colored screen, which is then normalized and transformed to tristimulus value $\tilde{T}_W$. Finally, the appearances of the image are transformed back using $\tilde{T}_W$ as the white point. Unlike the method in Section 3.1, however, since human eyes would not completely adapt to the screen color, we should not shift the input colors entirely toward it but only by a small amount. To fulfill the job, the adaptation degree factor F in the CIECAM02 model is utilized. F determines the degree the output appearances adapt to the white point. It can be set to 0 for no adaptation, or to 1 for complete adaptation. By changing F, the amount of hue adjustment can be controlled. In our algorithm, it is also determined through an optimization process.

3.3. Simplification

Since both brightness scaling and hue adjustment take advantage of the CIECAM02 model, they can be combined into one transformation, thus reducing half of the work. In this new transformation, the luminance values of the image would be transformed to appearances using T_W as the white point and then be transformed back using $\alpha\tilde{T}_W$ as the white point.

Using the CIECAM02 model is computationally heavy. Because only the anchor is replaced between the forward and the backward transformation, some approximations are utilized in our algorithm to simplify the process. The flow of the original model can be found in [16], and since the following notations accord with those in [16], they will not be introduced again here. In the forward conversion, the color in the reference illuminant can be approximated as

$$R_c = \left(\frac{Y_w}{R_w}D + 1 - D\right)R \cong (1-D)R, \qquad (1)$$

which can also be applied on G_c and B_c. For the following, we will only take R_c for example. Then, the response in Hunt–Pointer–Estévez space and its compression are

$$\begin{bmatrix} R' \\ G' \\ B' \end{bmatrix} = M_H M_{CAT02}^{-1} \begin{bmatrix} R_c \\ G_c \\ B_c \end{bmatrix} \cong (1-D) M_H \begin{bmatrix} X \\ Y \\ Z \end{bmatrix}, \quad (2)$$

$$R'_a = \frac{400(F_L R'/100)^{0.42}}{27.13+(F_L R'/100)^{0.42}} + 0.1 \cong \frac{400}{27.13}(F_L R'/100)^{0.42}, \quad (3)$$

$$A = \left(2R'_a + G'_a + \frac{1}{20}B'_a - 0.305\right)N_{bb} \cong \left(2R'_a + G'_a + \frac{1}{20}B'_a\right)N_{bb}. \quad (4)$$

Finally, the lightness can be approximated as

$$\begin{aligned} J &= 100\left(\frac{A}{A_w}\right)^{cz} \cong 100\left(\frac{2R'_a + G'_a + B'_a/20}{2R'_{wa} + G'_{wa} + B'_{wa}/20}\right)^{cz} \\ &\cong 100\left(\frac{2(R'_a/R'_{wa}) + (G'_a/G'_{wa}) + (B'_a/B'_{wa})/20}{2+1+1/20}\right)^{cz} \\ &\cong 100\left(\frac{2(R'/R'_w)^{0.42} + (G'/G'_w)^{0.42} + (B'/B'_w)^{0.42}/20}{3+1/20}\right)^{cz}. \end{aligned} \quad (5)$$

In the backward conversion, assume

$$\tilde{Y}_w = kY_w, \quad (6)$$

where $\tilde{Y}_w$ represents the Y component of the new white point. In this part, all variables with a tilde denote values derived in the backward process, i.e., from the new white point. For the achromatic response $\tilde{A}_w$ of the new white point, since it only needs to be calculated once instead of for each pixel, it is calculated in exact form. Let the ratio of $\tilde{A}_w / A_w$ be β, then

$$\tilde{A} = \tilde{A}_w \left(\frac{J}{100}\right)^{1/c\tilde{z}} = \beta \left(\frac{J}{100}\right)^{1/c\tilde{z}-1/cz} A = \gamma A, \quad (7)$$

where $\gamma = \beta(J/100)^{1/c\tilde{z}-1/cz}$. Then the correlate for red-green $\tilde{a}$ and correlate for yellow-blue $\tilde{b}$ can then be calculated as

$$\tilde{p}_1 = \frac{50000}{13} N_c \tilde{N}_{cb} \frac{e_t}{\tilde{t}} = \frac{\tilde{N}_{cb}}{N_{cb}} \frac{t}{\tilde{t}} p_1 = \left(\frac{\tilde{Y}_w}{Y_w}\right)^{0.2} \frac{t}{\tilde{t}} p_1 = k^{0.2} \frac{t}{\tilde{t}} p_1, \quad (8)$$

$$\tilde{p}_2 = \tilde{A}/\tilde{N}_{bb} + 0.305 = \frac{\tilde{A}/\tilde{N}_{bb} + 0.305}{A/N_{bb} + 0.305} p_2 \cong k^{-0.2} \gamma p_2, \quad (9)$$

$$\tilde{t} = \left(\frac{1.64 - 0.29^n}{1.64 - 0.29^{n/k}}\right)^{0.8111} t \cong k^{0.2} t, \quad (10)$$

$$\tilde{b} = \frac{c\tilde{p}_2}{\tilde{p}_1 \csc h + d \cot h + f} \cong \frac{\tilde{p}_2}{p_2} \frac{p_1}{\tilde{p}_1} b = k^{-0.4} \frac{\tilde{A}}{A} \frac{\tilde{t}}{t} b \cong k^{-0.2} \gamma b, \quad (11)$$

$$\tilde{a} = \tilde{b} \cot h = k^{-0.2} \gamma a. \quad (12)$$

Thus the responses in Hunt–Pointer–Estévez space and its compression are

$$\begin{bmatrix} \tilde{R}'_a \\ \tilde{G}'_a \\ \tilde{B}'_a \end{bmatrix} = \begin{bmatrix} 2 & 1 & 1/20 \\ 1 & -12/11 & 1/11 \\ 1/9 & 1/9 & -2/9 \end{bmatrix}^{-1} \begin{bmatrix} \tilde{p}_2 \\ \tilde{a} \\ \tilde{b} \end{bmatrix} \cong k^{-0.2} \gamma \begin{bmatrix} R'_a \\ G'_a \\ B'_a \end{bmatrix}, \quad (13)$$

$$\tilde{R}' = \left(\frac{-27(\tilde{R}'_a - 0.1)}{\tilde{R}'_a - 400.1}\right)^{\frac{1}{0.42}} \frac{100}{F_L} \cong \left(\frac{\tilde{R}'_a}{R'_a}\right)^{\frac{1}{0.42}} R' \cong \left(\frac{\gamma}{k^{0.2}}\right)^{\frac{1}{0.42}} R'. \quad (14)$$

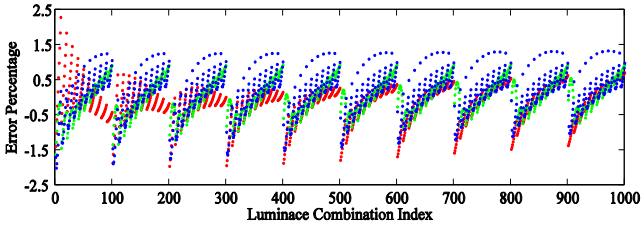

Fig. 2. Error percentages for different luminance combinations when the approximation is adopted. The R/G/B dots represent the errors of R/G/B channels, respectively. It can be seen that all errors are within ±2.5%.

Finally, the new tristimulus values can be approximated as

$$\begin{bmatrix} \tilde{R}_c \\ \tilde{G}_c \\ \tilde{B}_c \end{bmatrix} \cong M_{CAT02} M_H^{-1} \begin{bmatrix} \tilde{R}' \\ \tilde{G}' \\ \tilde{B}' \end{bmatrix} \cong \left(\frac{\gamma}{k^{0.2}}\right)^{1/0.42} \begin{bmatrix} R_c \\ G_c \\ B_c \end{bmatrix}, \quad (15)$$

$$\tilde{R} = \tilde{R}_c / \left(\frac{Y_w D}{\tilde{R}_w} + 1 - D\right) \cong \left(\frac{\gamma}{k^{0.2}}\right)^{\frac{1}{0.42}} \frac{100D/R_w + 1 - D}{100D/\tilde{R}_w + 1 - D} R. \quad (16)$$

By using the above approximations, the time complexity of using the CIECAM02 model can be reduced dramatically. To verify its feasibility, it was tested on normalized luminance values from [0.1, 0.1, 0.1] to [1, 1, 1] (0.1 for each step, total 1000 combinations). The error percentages with respect to the exact solutions for α = 0.1, F = 0.02 are shown in Fig. 2.

3.4. Optimization Framework

Recall that in our work, $\alpha \tilde{T}_W$ was used as the new white point, and F is the adaptation degree. To determine the values of α and F, an optimization process is performed,

$$(\alpha, F) = \arg\min_{\alpha,F} \left\{ w_1 \left[(1-\alpha)^2 + w_2 F^2 \right] + E_u \right\}, \quad (17)$$

where w_1 and w_2 are the weights for α and F, respectively, and E_u is the over-upper-bound error of the resulting image,

$$E_u = \sum_i 1\{p_i > U\}(p_i - U)^2 / |I|, \quad (18)$$

where $1\{\bullet\}$ denotes the indicator function, p_i is the luminance value of pixel i, U is the upper bound of the projector's dynamic range, and $|I|$ denotes the image size in number of pixels. This framework tries to preserve the image brightness (α) while repressing the hue adjustment amount (F) and pixel saturations (E_u).

To test the luminance benefit the anchoring theory can bring us, the proposed framework was applied to various mono-color images when projected on a magenta screen, with their hues varying from 10 to 360 (10 for each step) and chroma varying from 25 to 100 (25 for each step). Then we fixed F in (17) and set w_1 to 10^4 to solve for α. The ratios of the resulting α when F = 0.02 to F = 0 (i.e., no anchoring theory applied) are shown in Fig. 3. It can be seen that when the image color is away from the color of the screen, the α gains remain nearly constant. To better prove its robustness, the above procedure was also applied to 44 test images selected from various image sets including Waterloo [17], Kodak [18] and SIPI [19]. The ratios of the resulting α when

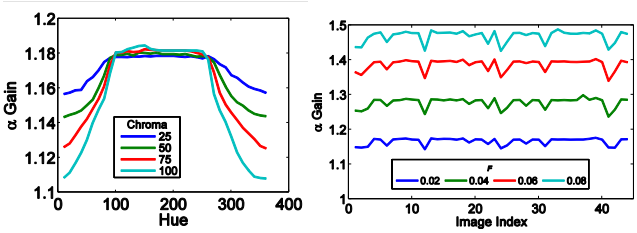

Fig.3. The α gains of different mono-colored images (left) and the α gains of different test images (right) on a magenta screen.

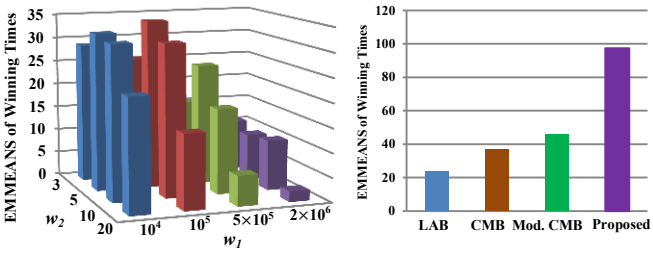

Fig. 4. The EMMeans of the winning times of different combinations of w_1 and w_2 (left) and of different algorithms (right).

F was set to different values to the results when $F = 0$ are also shown in Fig. 3. Again the α gains remain nearly constant when F is fixed, which shows the algorithm's stability.

3.5. Parameter Determination

A subjective test including 20 subjects was conducted to determine the values of w_1 and w_2. Since these two parameters are continuous and cannot be tested for all possible values, we chose four values of w_1 and four values of w_2 as candidates, and tested these 16 combinations on 10 out of the 44 test images. In the test, the subject would see the original image projected on the white screen and two out of the sixteen compensated image alternatively projected on the colored screen, which the subject could switch between rapidly. After enough observations, the subject would be asked to choose the one that resembled the original image more. The one that won would be remained for the following competitions, while the lost one would be eliminated. For each round, the compensated images would be selected at random to eliminate any biase choices. An ANOVA (Analysis of Variance) was conducted on the total numbers of the winning times of each combination, and the estimated marginal means (EMMEANS) are shown in Fig. 4. It can be seen that the performance is the best when $w_1 = 10^5$ and $w_2 = 5$, so this was selected as the final choice as an approximation of the optimal point.

4. EXPERIMENTS

A subjective test including 10 subjects was conducted on the remaining 34 test images to compare the proposed method with three other algorithms: the LAB algorithm, the CMB algorithm [13], and the modified CMB algorithm. The LAB algorithm tries to find the closest match in the CIE $L^*a^*b^*$ space for each pixel when reducing the image brightness, and the modified CMB algorithm replaces the over-upper-bound-error in [13] with (18) to compute the optimal solution. The same procedure used to determine the parameters was again adopted to conduct the experiment, but this time, all possible comparisons were performed. To verify the reliability, we again tested the results with ANOVA, and the EMMEANS of the winning times for each algorithm are also shown in Fig. 4. It turned out that for all pairs, a difference is observed for a confidence level of 99%. Besides, the proposed algorithm won for nearly all comparisons with the others (974/1020). A sample visual result is shown in Fig. 5.

Fig. 5. Comparison of different compensation algorithms. Note that (f) has better contrast and closer raft color to the original's. Since the response curves of the camera and the display alter the screen color from that directly seen by human eyes, the effect of chroma adaptation may not be well pronounced here. However, its existence can still be verified by the subjective test.

5. CONCLUSION

In this paper, we have described a method based on the anchoring theory to improve the luminance-scaling of a procam system when an image is projected on a colored screen. It has three notable features. First, unlike previous methods that use a linear approach, the proposed method takes the nonlinear characteristic of human eyes into consideration. Second, the method accounts for the chromatic adaptation property of HVS. Finally, the computational framework developed in this work strikes a balance between chroma distortion and brightness loss. As a result, the perceptual quality of the compensated image is significantly improved, which can be evidenced by the subjective test.

6. REFERENCES

[1] M. D. Grossberg, H. Peri, S. K. Nayar, and P. N. Belhumeur, "Making one object look like another: controlling appearance using a projector-camera system," in *Proc. CVPR*, vol. 1, pp. 452-459, 2004.

[2] O. Bimber, A. Emmerling, and T. Klemmer, "Embedded entertainment with smart projectors," *IEEE Computer*, vol. 38, pp. 48-55, 2005.

[3] D.–C. Kim, T.–H. Lee, M.–H. Choi, and Y.–H. Ha, "Color correction for projected image on colored screen based on a camera," in *Proc. SPIE*, vol. 7866, 2011.

[4] A. Majumder and R. Stevens, "LAM: Luminance attenuation map for photometric uniformity in projection based displays," in *Proc. ACM VRST*, pp. 147-154, 2002.

[5] A. Majumder, D. Jones, M. McCrory, M. E. Papka, and R. Stevens, "Using a camera to capture and correct spatial photometric variation in multi-projector displays," in *Proc. IEEE PROCAMS*, 2003.

[6] A. Majumder and M. S. Brown, "Building large area displays," *Eurographics*, 2003.

[7] D. Wang, I. Sato, T. Okabe, and Y. Sato, "Radiometric compensation in a projector-camera system based on the properties of human vision system," in *Proc. CVPR*, vol. 3, 2005.

[8] A. Majumder and R. Stevens, "Perceptual photometric seamlessness in projection-based tiled displays," *ACM Transactions on Graphics*, vol. 24, pp. 118–139, 2005.

[9] M. Ashdown, T. Okabe, I. Sato, and Y. Sato, "Robust content-dependent photometric projector compensation," in *Proc. IEEE PROCAMS*, 2006.

[10] O. Bimber, D. Iwai, G. Wetzstein, and A. Grundhöfer, "The visual computing of projector-camera systems," *Eurographics*, 2007

[11] W. Zou and H. Xu, "Colorimetric color reproduction framework for screen relaxation of projection display," *Displays*, vol. 32, pp. 313-319, 2011.

[12] B. Zhu, L. Xie, T. Yang, Q. Wang, and Y. Zheng, "A novel radiometric projector compensation algorithm based on Lambertian reflection model," in *Proc. SPIE,* vol. 8004, 2011.

[13] T.-H. Huang, C.-T. Kao, and H. H. Chen, "Quality enhancement of procam system by radiometric compensation," in *Proc. IEEE MMSP*, pp. 192-197, 2012.

[14] M.D. Fairchild, *Color Appearance Models*, 2nd Ed., Wiley-IS&T, Chichester, UK, 2005.

[15] A. Gilchrist, *et al.,* "An anchoring theory of lightness perception," *Psych. Rev.,* vol. 106, pp. 795–834, 1999.

[16] N. Moroney, M.D. Fairchild, R.W.G. Hunt, C.J. Li, M.R. Luo, and T. Newman, "The CIECAM02 color appearance model," in *Proc. IS&T/SID 10th Color Imaging Conference*, pp. 23-27, 2002.

[17] G. Mayer. (2012) Waterloo image repository. [Online]. Available: http://links.uwaterloo.ca/Repository.html/

[18] R. Franzen. (2012) Kodak lossless true color image suite. [Online]. Available: http://r0k.us/graphics/kodak/

[19] A. Weber. (2012) The USC-SIPI image database. [Online]. Available: http://sipi.usc.edu/database/database.php/